



Strathprints Institutional Repository

Eliasson, B. and Leyser, T. B. (2015) Numerical study of upper hybrid to Z mode leakage during electromagnetic pumping of groups of striations in the ionosphere. *Annales Geophysicae*, 33. pp. 1019-1030. ISSN 0992-7689 , <http://dx.doi.org/10.5194/angeo-33-1019-2015>

This version is available at <http://strathprints.strath.ac.uk/54012/>

Strathprints is designed to allow users to access the research output of the University of Strathclyde. Unless otherwise explicitly stated on the manuscript, Copyright © and Moral Rights for the papers on this site are retained by the individual authors and/or other copyright owners. Please check the manuscript for details of any other licences that may have been applied. You may not engage in further distribution of the material for any profitmaking activities or any commercial gain. You may freely distribute both the url (<http://strathprints.strath.ac.uk/>) and the content of this paper for research or private study, educational, or not-for-profit purposes without prior permission or charge.

Any correspondence concerning this service should be sent to Strathprints administrator: strathprints@strath.ac.uk

Numerical study of upper hybrid to Z mode leakage during electromagnetic pumping of groups of striations in the ionosphere

B. Eliasson¹ and T. B. Leyser²

¹SUPA, Physics Department, John Anderson Building, Strathclyde University, Glasgow G4 0NG, Scotland, UK.

²Swedish Institute of Space Physics, Box 537, SE-751 21 Uppsala, Sweden

Correspondence to: B. Eliasson (bengt.eliasson@strath.ac.uk)

Abstract. We investigate numerically the interaction between ionospheric magnetic field-aligned density striations and a left-hand circularly polarized (L) mode wave. The L mode wave is scattered into upper hybrid (UH) waves which are partially trapped in the striations, but are leaking energy to electromagnetic waves in the Z mode branch. For small amplitude (1%) striations, this loss mechanism leads to a significant reduction in amplitude of the UH waves. For several striations organized in a lattice, the leaking of Z mode waves is compensated by influx of Z mode radiation from neighboring striations, leading to an increased amplitude of the weakly trapped UH waves. For large amplitude (10%) striations the trapped UH waves rapidly increase in amplitude far beyond the threshold for parametric instabilities, and the Z mode leakage is less important. The results have relevance for the growth of striations and the onset of UH and lower hybrid turbulence during electromagnetic high frequency pumping of ionospheric plasma, which require large amplitude UH waves.

1 Introduction

Powerful electromagnetic high frequency (HF) waves transmitted into the ionosphere excite geomagnetic field-aligned plasma density striations. The structuring in the plasma into striations absorbs substantial power from the injected pump wave when it has ordinary (O) mode polarization and its frequency is below the maximum upper hybrid (UH) frequency of the ionosphere (Cohen and Whitehead, 1970; Stubbe et al., 1982; Mjølhus, 1985, 1998). Typical transverse (to the magnetic field) sizes of small-scale striations are a few meters up to tens of meters while their parallel sizes are tens of kilometers due to the strongly anisotropic mobility of the electrons in the magnetic field (Kelley et al., 1995; Franz et al., 1999). The striations are typically associated with local density depletions of the order 5–10%, and are observed to be separated by a few tens of meters. In situ measurements at Arecibo it was found that the spatial structure of the plasma density at large scales across the magnetic field is due to organization of the small-scale striations into bunches of a few

25 hundred meters across (Franz et al., 1999; Gurevich et al., 1998). At high latitudes, optical emissions
show self-organization into filaments of a few kilometers across during pumping in magnetic zenith
(Kosch et al., 2007; Leyser and Nordblad, 2009).

The small-scale striations result from pump-driven UH waves, which as the thermal instability
develops become self-localized in the density depletions of the striations (Vas'kov and Gurevich,
30 1976; Inhester et al., 1981; Vas'kov and Gurevich, 1984; Gurevich et al., 1995a; Istomin and Leyser,
1997). This occurs at altitudes where the pump frequency is below the UH frequency outside the
plasma depletion but above the local UH frequency in a region inside the depletion. Large amplitude
UH waves are excited at altitudes where the resonance frequency of the trapped UH waves equals
the transmitted frequency (Dyste et al., 1982; Mjølhus, 1998; Eliasson and Papadopoulos, 2015).
35 However, it is theoretically predicted that the localized UH oscillations are not perfectly trapped in
the depletions but radiate electromagnetic waves in the Z mode branch that escape from the striations
(Dyste et al., 1982; Mjølhus, 1983).

The electromagnetic interaction of several striations was first studied in the Wentzel–Kramers–
Brillouin (WKB) approximation for the localized UH field, which showed that the coupling depends
40 crucially on the phasing of the mean Z mode wave between the striations (Mjølhus, 1983). One-
dimensional theory predicts that the Z mode leakage from a single striation is so strong that a stri-
ation cannot be excited with presently available pump transmitter powers (Gurevich et al., 1995b).
However, it is proposed that in a system of parallel striations there would be partial influx of Z mode
waves to a given depletion from neighboring striations, to partly compensate for the Z mode leak-
45 age and thus enable excitation of striations with the available pump power. It has been proposed
(Gurevich et al., 1996) that for a system of about 40 striations, the total Z mode leakage and the
damping by collisions are of the same order.

Using a scale separation technique, the amplitude of the Z mode wave has been obtained ana-
lytically in terms of eigenfunctions of the localized UH field in a single density depletion in one
50 dimension (Hall and Leyser, 2003). Several scattering processes are included. The electromagnetic
ordinary mode pump wave scatters off the density depletion into localized UH oscillations. For a
symmetric striation in one dimension, the pump wave only excites UH modes with the wave electric
field being an even function in space, while odd modes are not excited (Mjølhus, 1998). The UH
oscillations in turn scatter off the cavity into Z mode waves, which also can scatter off the depletion
55 into localized UH oscillations. The theory (Hall and Leyser, 2003) also includes the scattering of the
pump wave directly into Z mode waves on the density depletion. For a system of density cavities
(Istomin et al., 2006; Hall et al., 2009), the scattering of the pump wave directly into Z mode waves
leads to the excitation of odd UH modes for an asymmetric distribution of one-dimensional cavities,
although the original pump field and the depletions are symmetric. The system of striations is thus
60 electromagnetically coupled by the radiation of Z mode waves out from the striations and the influx

from neighboring striations and the strongly inhomogeneous UH turbulence is embedded in a sea of Z mode waves.

However, in ionospheric radio wave experiments the transverse profiles of the striations are believed to be two-dimensional and axisymmetric, rather than one-dimensional. As this case corresponds to odd UH resonances in one dimension, the analytic one-dimensional results has been used for a first two-dimensional treatment. It is predicted that the Z mode leakage is significantly weaker for a two-dimensional distribution of parallel striations compared to the one-dimensional case (Istomin et al., 2006; Hall et al., 2009). This is because the odd UH modes in two dimensional cavities correspond to dipole distributions of the localized fields while the even modes in the one-dimensional case correspond to monopole field distributions. The weaker dipole radiation of the UH field compared to the monopole radiation of even modes results in weaker Z mode leakage and therefore larger UH amplitude in the two-dimensional case.

The aim of this paper is to investigate numerically the linear mode conversion of an O mode wave to UH waves on clusters of two-dimensional striations, and how the leakage of Z mode waves affects the amplitude of the trapped UH waves. Both large and small amplitude striations are considered, and the influence of the size of striation clusters on the amplitude of the trapped UH waves is investigated. Section II describes the mathematical model used in the numerical work. The properties of trapped electrostatic UH oscillations in a single striation are discussed in Section III, while the coupling to Z mode waves in clusters of striations are numerically investigated in Section IV. Finally, the results are discussed and conclusions are drawn in Section V.

2 Mathematical model

An O mode polarized continuous wave injected into the overhead ionosphere along the magnetic field lines will excite UH resonances at quantized heights (Mjølhus, 1998; Eliasson and Papadopoulos, 2015) where the transmitted frequency matches one of the local resonances of the UH waves trapped in the striations. This leads to the excitation of large amplitude UH waves and to anomalous absorption of the O mode wave. When an O mode wave propagates parallel to the ambient magnetic field, it is in the form of a left-hand circularly polarized (L) mode wave with its electric field directed perpendicularly to the ambient magnetic field. For simplicity we do not take into account the effects of the vertical stratification of the plasma on the propagation of the L mode or on the interaction with the striations. The L mode wave is instead represented by an externally imposed left-hand polarized dipole electric field $\tilde{\mathbf{E}}_L = \tilde{E}_L(\hat{\mathbf{x}} - i\hat{\mathbf{y}})$, where $\hat{\mathbf{x}}$ and $\hat{\mathbf{y}}$ are unit vectors in the x - and y -directions. We use a two-dimensional simulation geometry in the x - y plane, transverse to the ambient magnetic field $\mathbf{B}_0 = \hat{\mathbf{z}}B_0$, where $\hat{\mathbf{z}}$ is the unit vector along the z -axis. The simulation box size is 200 m in both the x - and y -directions for simulations using 1 striation, while somewhat larger box sizes of 250 m and 300 m, respectively, are used for clusters of 7 and 19 striations (cf. Fig. 3 below). A pseudo-spectral

method is used to calculate derivatives in space accurately, and a 4th-order Runge-Kutta scheme is used to advance the solution in time.

Superimposed on the background electron and ion density are magnetic field aligned small-scale striations that are associated with localized density depletions at a fraction of the background density.

100 The total ion density is of the form $n(\mathbf{r}) = n_0 + n_s(\mathbf{r})$, where

$$n_s(\mathbf{r}) = -\alpha n_0 \sum_j \exp \left[-\frac{(x-x_j)^2}{D_{str}^2} - \frac{(y-y_j)^2}{D_{str}^2} \right] \quad (1)$$

describes the ion density profiles of the striations, (x_j, y_j) is the central position of each striation, α is the relative amplitude, n_0 is the background ion number density, and D_{str} is the transverse size of the striations.

105 The physics involves very disparate length-scales. The typical transverse size D_{str} is a few meters, while the electromagnetic wave with a frequency of a few MHz has a local wavelength of a few tens of meters, and UH waves trapped in the striations can have wavelengths of about a meter or less. For the electromagnetic model, the different length-scales pose a challenge on the numerical scheme, which has to resolve both the large and small scales, while using a sufficiently short
110 time-step Δt to maintain stability due to the Courant condition determined by the smallest scale, $\Delta t \lesssim \Delta x/c = \Delta y/c$, where Δx and Δy are the grid sizes in the x - and y -directions, and c is the speed of light in vacuum. The wavenumber, and hence the wavelength can be estimated by using the UH dispersion relation. At the center of the large amplitude striations used in the numerical work, the electron density is 90% of the ambient density, and therefore at the bottom of the striation,
115 where the upper hybrid waves have the shortest wavelength, we can use the dispersion relation $\omega^2 = 0.9\omega_{pe}^2 + \omega_{ce}^2 + 3v_{Te}^2\kappa k^2$ for the wave frequency ω , the electron plasma frequency ω_{pe} , electron cyclotron frequency ω_{ce} , electron thermal speed v_{Te} , wavenumber k and a kinetic correction coefficient κ (defined below). Using, for example, the frequency equal to the ambient UH frequency outside the striation, $\omega^2 = \omega_{pe}^2 + \omega_{ce}^2$, and eliminating ω , we obtain $0.1\omega_{pe}^2 = 3v_{Te}^2\kappa k^2$.
120 For the simulation parameters $\omega_{pe} = 20.12 \times 10^6$, $v_{Te} = 2.46 \times 10^5$ m/s, and $\kappa \approx 2.5$, we solve for the wavenumber to obtain $k \approx 9.4 \text{ m}^{-1}$, corresponding to an upper hybrid wavelength of 0.67m. In order to resolve the UH waves with more than two grid points per wavelength, the grid sizes are set to $\Delta x = \Delta y = 0.2 \text{ m}$ in all simulations except in Figs. 4 and 7, where $\Delta x = \Delta y = 0.4 \text{ m}$ were used since the wave frequency was below the UH frequency and the wavelengths were longer. The
125 small grid-size puts a limit on the time-step. To relax the Courant condition, we here follow the strategy outlined by Eliasson (2013) and use a coarser resolution for the electromagnetic wave. In doing so, the electric field $\mathbf{E} = \mathbf{E}_{ES} + \mathbf{E}_{EM}$ is divided into one curl-free part $\mathbf{E}_{ES} = -\nabla\phi$ primarily associated with electrostatic waves, and one divergence free part $\mathbf{E}_{EM} = -\partial\mathbf{A}/\partial t$ associated with electromagnetic waves, where ϕ and \mathbf{A} are the scalar and vector potentials, respectively, and
130 using the Coulomb gauge $\nabla \cdot \mathbf{A} = 0$. High Fourier components of the electromagnetic field \mathbf{E}_\perp and \mathbf{A} , corresponding to the wave vector components k_x and k_y having magnitudes larger than a

maximum wavenumber k_{\max} , are set to zero. This corresponds effectively to representing the solution on a coarser grid $\Delta\bar{x} = \Delta\bar{y} = \pi/k_{\max}$. In order to resolve the electromagnetic wave, the value of k_{\max} has to be larger than the typical wavenumber of the electromagnetic wave. We choose
135 $k_{\max} \approx 0.8 \text{ m}^{-1}$, while the shortest wavelength of the Z mode in the simulations is 15 m, corresponding to a wavenumber of 0.4 m^{-1} , and hence the electromagnetic wave is well resolved. The effective coarser grid size is $\Delta\bar{x} = \Delta\bar{y} = \pi/k_{\max} \approx 4 \text{ m}$, and we can use about 10 times longer time steps, making the simulations feasible on a standard single processor workstation. The time-step used in the simulations using the electromagnetic models is $\Delta t = 5 \times 10^{-9} \text{ s}$, while for simulations
140 using an electrostatic model, the time-step is essentially limited by the inverse of the upper hybrid frequency and is taken to be $\Delta t = 5 \times 10^{-8} \text{ s}$.

The HF component of the electric field is assumed to take the form $\mathbf{E} = (1/2)(\tilde{\mathbf{E}}(z, t) \exp(-i\omega_0 t) + \tilde{\mathbf{E}}^*(z, t) \exp(i\omega_0 t))$, where $\tilde{\mathbf{E}}$ represents the slowly varying complex envelope of the HF field, and ω_0 is the transmitted frequency of the L mode wave, and the asterisk denotes complex conjugation.
145 Similar assumptions are made for the HF magnetic field, scalar potential, and the electron density and velocity fluctuations, which are linearly coupled to the HF electric field. Hence, the time derivatives on the fast timescale are transformed as $\partial/\partial t \rightarrow \partial/\partial t - i\omega_0$ in the governing equations for the envelopes of the HF fields. We assume that the HF current is carried by the electrons, while the ions are stationary and contribute only to the neutralizing background and to the density profiles of the
150 striations. The complex-valued envelopes of the electromagnetic fields are then obtained from the linearized evolution equations

$$\frac{\partial \tilde{\mathbf{A}}}{\partial t} = i\omega_0 \tilde{\mathbf{A}} - \tilde{\mathbf{E}}_{EM} \quad (2)$$

and

$$\frac{\partial \tilde{\mathbf{E}}_{EM}}{\partial t} = i\omega_0 \tilde{\mathbf{E}}_{EM} - c^2 \nabla^2 \tilde{\mathbf{A}} - \frac{e}{\varepsilon_0} \nabla^{-2} \nabla \times [\nabla \times (n \tilde{\mathbf{v}}_e)], \quad (3)$$

155 where e is the magnitude of the electron charge and ε_0 is the electric vacuum permittivity. Here, ∇^{-2} denotes the inverse of the Laplacian operator, which is efficiently calculated in Fourier space using a pseudospectral method. The envelope of the electrostatic field is $\tilde{\mathbf{E}}_{ES} = -\nabla \tilde{\phi}$, where the scalar potential $\tilde{\phi}$ is obtained from Poisson's equation

$$\nabla^2 \tilde{\phi} = \frac{e}{\varepsilon_0} \tilde{n}_e. \quad (4)$$

160 The HF electron dynamics is governed by the electron continuity and momentum equation

$$\frac{\partial \tilde{n}_e}{\partial t} = i\omega_0 \tilde{n}_e - \nabla \cdot (n \tilde{\mathbf{v}}_e) \quad (5)$$

and

$$\frac{\partial \tilde{\mathbf{v}}_e}{\partial t} = i\omega_0 \tilde{\mathbf{v}}_e - \frac{e}{m_e} \left(\tilde{\mathbf{E}} + \tilde{\mathbf{E}}_L + \tilde{\mathbf{v}}_e \times \mathbf{B}_0 \right) - \frac{3v_{Te}^2}{n} \kappa \nabla \tilde{n}_e - \nu_e \tilde{\mathbf{v}}_e, \quad (6)$$

respectively, where $\tilde{\mathbf{E}} = \tilde{\mathbf{E}}_{ES} + \tilde{\mathbf{E}}_{EM}$ is the self-consistent electric field, m_e is the electron mass, ν_e is the effective electron collision frequency due to collisions with neutrals and ions, $v_{Te} = (k_B T_e / m_e)^{1/2}$ is the electron thermal speed, T_e is the electron temperature, and k_B is Boltzmann's constant. The coefficient $\kappa = \omega_0^2 / (\omega_0^2 - 4\omega_{ce}^2)$, where $\omega_{ce} = eB_0 / m_e$ is the electron cyclotron frequency, is a dispersive effect derived from kinetic theory (Lominadze, 1981; Istomin and Leyser, 2013), in which the UH wave is one of many electron Bernstein modes. For $\omega_0 < 2\omega_{ce}$, the UH wave changes topology and becomes a backward wave as part of the first electron Bernstein mode, and in this case the UH waves are not trapped in density depletions. We use $\omega_0 / \omega_{ce} \approx 2.5$ in the numerical treatment below. To absorb the escaping Z mode radiation, an absorbing layer is introduced near the boundaries; see Appendix A for details.

3 Trapped upper hybrid modes in a single striation

In the electrostatic limit, the system behaves as a Sturm-Liouville problem which allows a set of undriven standing UH wave trapped in the striations with resonance frequencies below the ambient UH frequency. To investigate these resonances, we employ Eqs. (4)–(6) in the electrostatic ($\tilde{\mathbf{E}}_{EM} = 0$ and $\tilde{\mathbf{A}} = 0$) and collision-less ($\nu_e = 0$) limits with no driving field ($\tilde{\mathbf{E}}_L = 0$). We assume the solution to be proportional to $\exp(i\delta\omega t)$, so that $\partial/\partial t \rightarrow -i\delta\omega$ where $\delta\omega$ is a frequency shift, and denote the total frequency $\omega = \omega_0 + \delta\omega$. Eliminating \tilde{n}_e and $\tilde{\mathbf{v}}_e$ from Eqs. (4)–(6) gives

$$3v_{Te}^2 \kappa \nabla^2 \tilde{\phi} + \omega^2 \left[\left(1 - Y^2 - X \frac{n}{n_0} \right) \tilde{\phi} - \tilde{\psi} \right] = 0 \quad (7)$$

where $X = \omega_{pe}^2 / \omega^2$, $Y = \omega_{ce} / \omega$, and $\tilde{\psi}$ is defined via

$$\nabla^2 \tilde{\psi} + X \left[\nabla \cdot \left(\frac{\nabla n}{n_0} \tilde{\phi} \right) + iY \hat{\mathbf{z}} \cdot \left(\frac{\nabla n}{n_0} \times \nabla \tilde{\phi} \right) \right] = 0. \quad (8)$$

In the ambient plasma where $n = n_0$, we have in the long wavelength limit $\nabla = 0$ so that $1 - Y^2 - X = 0$, or $\omega^2 = \omega_{UH}^2$, where $\omega_{UH} = (\omega_{pe}^2 + \omega_{ce}^2)^{1/2}$ is the UH resonance frequency and $\omega_{pe} = (n_0 e^2 / (\epsilon_0 m_e))^{1/2}$ is the electron plasma frequency. UH waves with $\omega < \omega_{UH}$ can be trapped in striations where $n < n_0$ locally in space (provided $\omega > 2\omega_{ce}$). In this case ω works as an eigenvalue for the set of eigenfunctions $\tilde{\phi}$ and $\tilde{\psi}$.

We next restrict the investigation to one cylindrically symmetric striation centered at $x = y = 0$. Introducing cylindrical coordinates $x = r \cos \theta$ and $y = r \sin \theta$, we assume that the potential is of the form $\tilde{\phi}(r, \theta) = \tilde{\Phi}(r) \exp(iN\theta)$ and $\tilde{\psi}(r, \theta) = \tilde{\Psi}(r) \exp(iN\theta)$, where $N = 0, \pm 1, \pm 2, \dots$ are azimuthal mode numbers, and the background plasma density $n(r)$ depends only on the radial coordinate r . Inserted into Eqs. (7) and (8), this leads to the system

$$\frac{3v_{Te}^2 \kappa}{r^2} \left[r \frac{\partial}{\partial r} \left(r \frac{\partial \tilde{\Phi}}{\partial r} \right) - N^2 \tilde{\Phi} \right] + \omega^2 \left[\left(1 - Y^2 - X \frac{n}{n_0} \right) \tilde{\Phi} - \tilde{\Psi} \right] = 0 \quad (9)$$

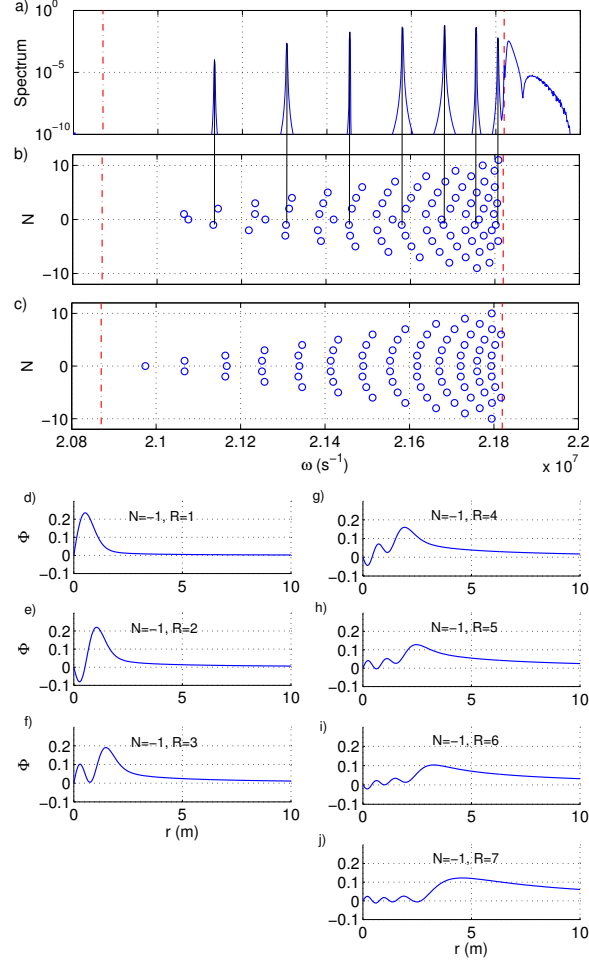


Figure 1. (a) The frequency spectrum of UH oscillations (arbitrary units) at the center of a deep striation ($\alpha = 0.1$), obtained from an electrostatic simulation using a short driving pulse at the beginning of the simulation to excite oscillations. (b)–(c): Resonances indicated by circles, showing the eigenfrequencies ω and azimuthal mode numbers N for (b) the coupled system (9)–(10), and (c) the Schrödinger equation (13). For each azimuthal mode number, there exist one or more radial modes enumerated by the mode number R with $R = 1$ having the lowest frequency. Small azimuthal mode numbers N are associated with larger numbers of radial modes. The vertical dash-dotted and dashed lines indicate the local UH frequency at the center of and outside the striation, respectively, and vertical solid lines connect the spectral peaks in (a) with the resonances for $N = -1$ in (b). (d)–(j): Spatial profiles (arbitrary units) of the radial eigenmodes $R = 1, \dots, 7$ for the azimuthal mode number $N = -1$ in panel (b) for trapped UH waves. The eigenmodes have the number of extrema equal to the radial mode number R .

195 and

$$r \frac{\partial}{\partial r} \left(r \frac{\partial \tilde{\Psi}}{\partial r} \right) - N^2 \tilde{\Psi} + X \left(r \frac{\partial}{\partial r} - YN \right) \left(\frac{r}{n_0} \frac{\partial n}{\partial r} \tilde{\Phi} \right) = 0. \quad (10)$$

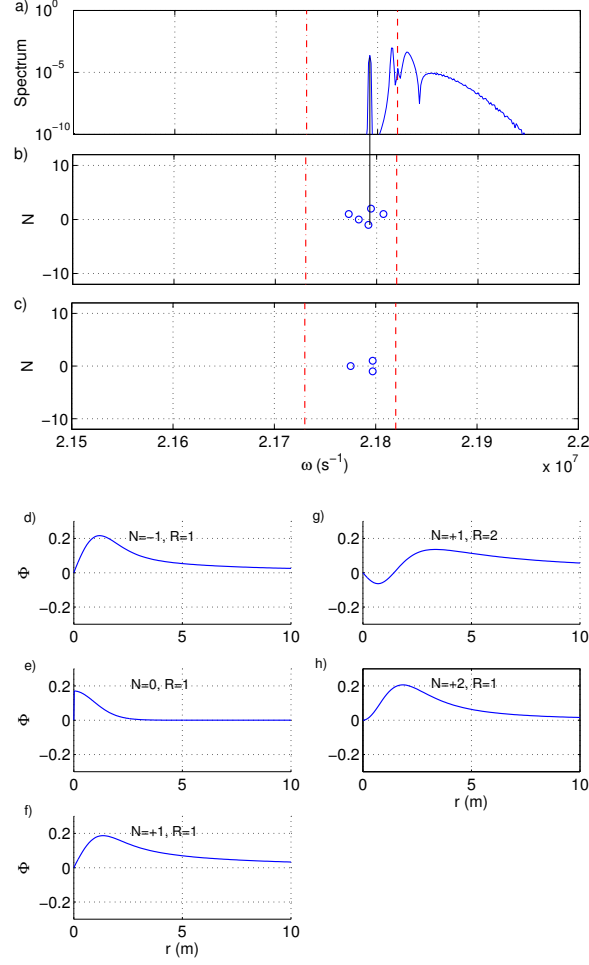


Figure 2. (a) The frequency spectrum (arbitrary units) of UH oscillations at the center of a shallow striation ($\alpha = 0.01$). (b)–(c): Resonances indicated by circles, showing the eigenfrequencies ω and azimuthal mode numbers N for (b) the coupled system (9)–(10) and (c) the Schrödinger equation (13). The vertical dash-dotted and dashed lines indicate the local UH frequency at the center of and outside the striation, respectively, and a vertical solid line connects a spectral peak in (a) with the resonance for $N = -1$ in (b). (d)–(h) Spatial profiles (arbitrary units) of the radial eigenmodes corresponding to the resonances [cf. panel (b)], for trapped UH waves.

The term proportional to YN in Eq. (10) shows that the symmetry is broken between positive and negative azimuthal mode numbers in the presence of an ambient magnetic field. Appropriate boundary conditions for $N \neq 0$ are $\tilde{\Phi} = 0$ and $\tilde{\Psi} = 0$ at $r = \infty$ and at $r = 0$. For $N = 0$, the boundary condition for Φ at $r = 0$ can be taken $\partial\tilde{\Phi}/\partial r = 0$, while Eq. (10) reduces to

$$\frac{\partial\tilde{\Psi}}{\partial r} + \frac{X}{n_0} \frac{\partial n}{\partial r} \tilde{\Phi} = 0, \quad (11)$$

and it is only possible to impose the boundary condition $\tilde{\Psi} = 0$ at $r = \infty$, giving

$$\tilde{\Psi} = \int_r^\infty \frac{X}{n_0} \frac{\partial n}{\partial r} \tilde{\Phi} dr, \quad (12)$$

which is used to eliminate $\tilde{\Psi}$ in Eq. (9).

205 To lowest order, neglecting terms containing derivatives of n (hence setting $\tilde{\Psi} = 0$), we have have from Eq. (9) the time-independent, cylindrical Schrödinger equation

$$\frac{3v_{Te}^2 \kappa}{r^2} \left[r \frac{\partial}{\partial r} \left(r \frac{\partial \tilde{\Phi}}{\partial r} \right) - N^2 \tilde{\Phi} \right] + \omega^2 \left(1 - Y^2 - X \frac{n}{n_0} \right) \tilde{\Phi} = 0, \quad (13)$$

which is a simplified model for trapped UH waves in a cylindrically symmetric striation.

The solution of the eigenvalue problem provides a set of eigenfrequencies $\omega = \omega_1, \omega_2, \dots$, and
 210 corresponding trapped waves for $\omega_j < \omega_{UH}$. By choosing the pump frequency equal to one of the resonances, $\omega_0 = \omega_j$, the respective UH mode is pumped resonantly. First, simulations of Eqs. (4)–(6) are carried out in the electrostatic limit ($\mathbf{E}_{EM} = 0$ and $\mathbf{A} = 0$) and are compared with solutions of the time-independent systems (9)–(12) and (13), and the results are presented in Figs. 1 and 2. Details of the numerical methods used to solve the time-independent equations are given in Appendix
 215 B. We consider one case of a deep striation with a relatively deep striation with $\alpha = 0.1$ (Fig. 1) and one case of a shallow striation with $\alpha = 0.01$ (Fig. 2). In both cases, the striation has the transverse size $D_{str} = 2$ m. We use the ambient plasma parameters $T_e = 4000$ K, $B_0 = 4.8 \times 10^{-5}$ T and $n_0 = 1.272 \times 10^{11}$ m $^{-3}$, giving $v_{Te} = 2.46 \times 10^5$ m/s, $\omega_{ce} = 8.44 \times 10^6$ s $^{-1}$, $\omega_{pe} = 20.12 \times 10^6$ s $^{-1}$, and $\omega_{UH} = 21.82 \times 10^6$ s $^{-1}$. We use $\kappa = 2.67$ in all cases. To excite UH oscillations in the simulations, a
 220 short driving pulse of the form $\tilde{E}_L(t) = E_{L0} \sin(\pi t / 2 \times 10^{-5})$ for $0 \leq t \leq 2 \times 10^{-5}$ s and $\tilde{E}_L(t) = 0$ for $t > 2 \times 10^{-5}$ s with frequency $\omega_0 = 21.35 \times 10^6$ s $^{-1}$ and the reference amplitude $E_{L0} = 1$ V/m is used to excite UH oscillations at the beginning of the simulations.

Figure 1a shows the spectrum of trapped electrostatic oscillations in a single deep striation with $\alpha = 0.1$. Here, the plasma density at the center of the striation is 10% lower than the ambient density,
 225 leading to the local plasma and UH frequencies $\omega_{pe} = 19.09 \times 10^6$ s $^{-1}$ and $\omega_{UH} = 20.87 \times 10^6$ s $^{-1}$, respectively. Hence, the frequencies of the trapped UH waves are clamped between 20.87×10^6 s $^{-1}$ and 21.82×10^6 s $^{-1}$, indicated by vertical dash-dotted and dashed lines in Figs. 1a–c. The total simulation time is 5 ms, which gives reasonable frequency resolution of the wave spectrum. The wave energy is concentrated to frequencies correlated with the eigenfrequencies (resonances) of the
 230 system (9)–(10) shown in Fig. 1b. As a comparison, the spectrum for the Schrödinger equation (13) is shown in Fig. 1c. The spectral peaks in Fig. 1a are closely aligned with the resonances corresponding to $N = -1$ of the system (9)–(10) in Fig. 1b, as indicated by vertical lines. The spatial profiles of the radial eigenmodes for the azimuthal mode number $N = -1$ are shown in Figs. 1d–i. Eigenmodes with higher radial mode numbers R correspond to higher eigenfrequencies (but below the ambient
 235 UH frequency), they have larger number of extrema, their largest amplitude is at the outer edge

of the striation, and they are less localized in space since their frequencies are closer to ω_{UH} . In a similar manner as for one-dimensional striations (Mjølhus, 1998), the number of resonances in two-dimensional striations can be roughly estimated (using the Schrödinger equation) as

$$M = \frac{1}{12\pi\kappa\lambda_{De}^2 n_0} \iint (-n_s) dx dy = \frac{\alpha D_{str}^2}{12\kappa\lambda_{De}^2}. \quad (14)$$

240 For the used plasma parameters $\alpha = 0.1$, $D_{str} = 2$ m, $\kappa = 2.67$, and $\lambda_{De} = 1.22 \times 10^{-2}$ m, we have $M = 84$, to be compared with the 82 and 81 resonances found in Fig. 1b and c, respectively. Hence, the number of trapped eigenmodes is relatively large and forms more or less a continuum of waves in the deep striation.

In contrast, the shallow striation has only a few resonances, as seen in Fig. 2b and c, and only 245 two peaks with $\omega < \omega_{UH}$ are visible in the frequency spectrum in Fig. 2a. For the shallow striation, the local plasma and UH frequencies at the center of the striation are $\omega_{pe} = 20.02 \times 10^6 \text{ s}^{-1}$ and $\omega_{UH} = 21.73 \times 10^6 \text{ s}^{-1}$, respectively. Hence, for this case the frequencies of the trapped UH waves are between $21.73 \times 10^6 \text{ s}^{-1}$ and $21.82 \times 10^6 \text{ s}^{-1}$, indicated by vertical dash-dotted and dashed lines in Fig. 2a–c. Visible in Fig. 2a are two discrete peaks for $\omega < \omega_{UH}$, roughly correlated with the resonances for $N = \pm 1$ in Fig. 2b, while a continuum of frequency components corresponding to un-trapped waves is visible in Fig. 2a for $\omega > \omega_{UH}$. The radial profiles of the trapped modes 250 in Fig. 2d–h are relatively extended in space since the resonance frequencies are close to ω_{UH} .

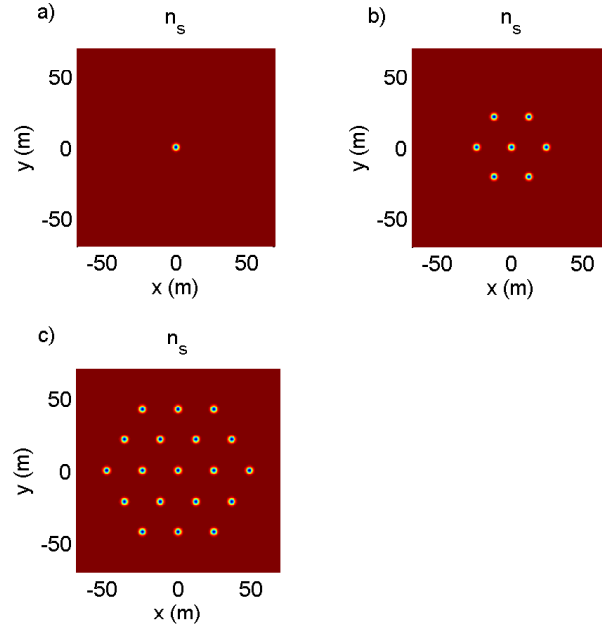


Figure 3. Close-ups of the density profiles associated with density striations for 1, 7 and 19 striations [panels (a)–(c)] organized in a hexagonal pattern in the x - y plane. The central distances between nearest neighbor striations is 24.53 m.

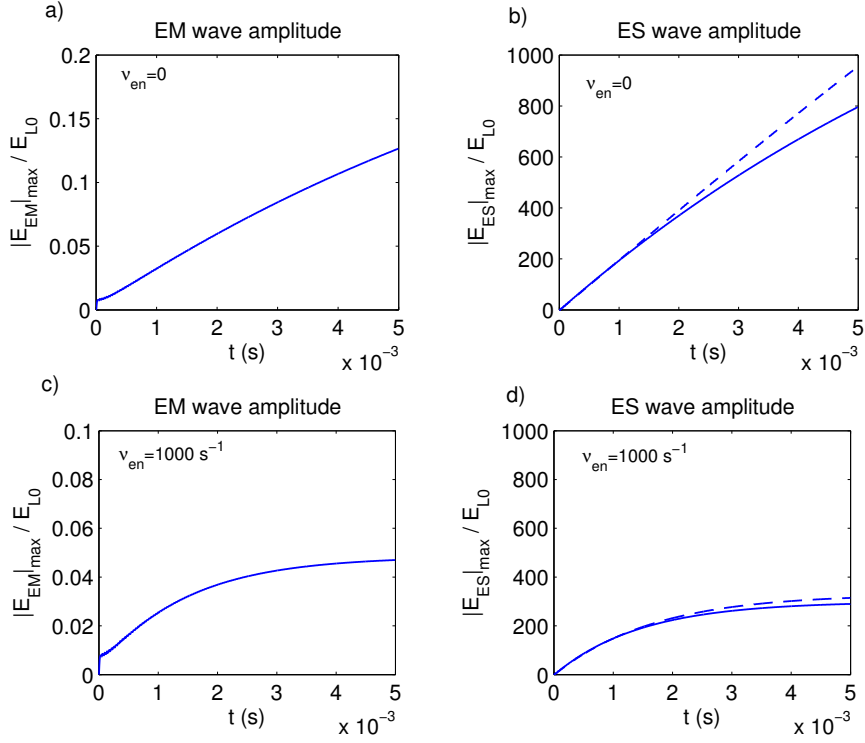


Figure 4. Simulations using a deep striation with $\alpha = 0.1$, excluding collisions (top) and including collisions with $\nu_e = 10^3 \text{ s}^{-1}$ (bottom), showing the electromagnetic (EM) field amplitude associated with Z mode waves [panels (a) and (c)] and electrostatic (ES) amplitude associated with UH waves [panels (b) and (d)]. The driving frequency ω_0 is set equal to resonant frequency $21.127 \times 10^6 \text{ s}^{-1}$ corresponding to the lowest radial mode for $N = -1$ and $R = 1$ in Fig. 1(b). The dashed lines in panels (b) and (d) show the result of electrostatic simulations.

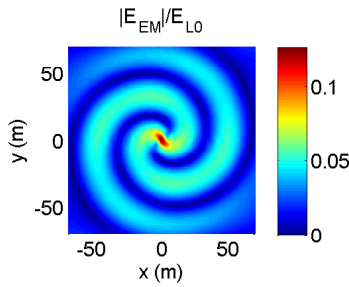


Figure 5. The amplitude of the electromagnetic waves at $t = 5 \text{ ms}$ for a deep striation with relative depth $\alpha = 0.1$, showing Z mode waves propagating away from the striation. The wavelength of the Z mode is $\lambda \approx 59.23 \text{ m}$ at frequency $\omega_0 = 21.127 \times 10^6 \text{ s}^{-1}$.

4 Coupling to Z mode waves in clusters of striations

We next carry out a set of simulations using a continuous wave (CW) driving L mode wave in clusters
 255 of striations to investigate the mode conversion of the L mode wave to UH waves, and the coupling
 to Z mode waves. Figure 3 shows the background ion number density for cases with 1, 7 and 19
 striations with transverse size $D_{str} = 2$ m, where groups of striations are organized in hexagonal
 patterns. The chosen central distance ≈ 25 m is consistent with the rocket experiment at Arecibo
 1992, where a rocket was flown through the heated region (Kelley et al., 1995; Franz et al., 1999).
 260 Franz et al. (1999) mention a mean spacing between the filaments across the magnetic field along
 the path of the satellite to be $s = 45$ m. This is roughly supported by the mean distance between
 filaments seen in their Fig. 1 and the one-dimensional spectrum in their Fig. 2 which has a spectral
 break at $k \approx 0.15 \text{ m}^{-1}$ corresponding to a perturbation wavelength of about 40 m. The mean width
 of the striations at half maximum was measured to be $w = 15$ m. Then the number of striations per
 265 unit area can be estimated to be $n_s = 1/(ws)$, and the mean distance between striations in the plane
 perpendicular to the magnetic field $d = 1/\sqrt{n_s} = \sqrt{ws} \approx 26$ m.

Figures 4 and 5 show the results of simulations using 1 deep striation with $\alpha = 0.1$. The reference
 amplitude of the L mode is $\tilde{E}_L = E_{L0} = 1$ V/m, and the driving frequency $\omega_0 = 21.127 \times 10^6 \text{ s}^{-1}$,
 corresponding to the resonance frequency for $N = -1$ and $R = 1$ in Fig. 1b. Simulations are carried
 270 out using the fully electromagnetic model and an electrostatic model (setting $\tilde{\mathbf{A}}$ and $\tilde{\mathbf{E}}_{\perp}$ to zero),
 and for cases without collisions ($\nu_e = 0$) and with collisions ($\nu_e = 10^3 \text{ s}^{-1}$). For the collision-less
 case (top panels in Fig. 4), the electrostatic field shown in Fig. 4b increases linearly with time to
 almost $10^3 E_{L0}$ at $t = 5$ ms. The simulations including collisions (bottom panels) show a saturation
 amplitude of the electrostatic field at about $300 E_{L0}$ (Fig. 4d). Figure 5 shows Z mode waves escaping
 275 the striation and propagating to the simulation boundaries where they are absorbed. By using the cold
 plasma dispersion relation for X mode waves,

$$c^2 k^2 = \frac{(\omega_0^2 - \omega_{pe}^2)^2 - \omega_{ce}^2 \omega_0^2}{\omega_0^2 - \omega_{UH}^2}, \quad (15)$$

the wavelength $\lambda = 2\pi/k$ of the escaping Z mode wave is estimated to be $\lambda \approx 59.23$ m. However, as
 seen in Fig. 4b and d, there is only a slight difference in the electrostatic wave amplitude between
 280 the electrostatic and fully electromagnetic simulations. Hence, for the deep striation, the Z mode
 leakage plays only a minor role for the UH amplitude, and collisions are more important. If the driv-
 ing L mode amplitude E_{L0} would be of the order 1 V/m, the UH wave amplitudes would rapidly
 exceed the threshold for nonlinearity, which is only a few V/m for ionospheric conditions. In a non-
 linear model, the large amplitude UH waves would excite parametric wave couplings to lower hybrid
 285 waves (see e.g. Ref. (Litvak et al., 1983) for laboratory conditions and Refs. (Gurevich et al., 1997;
 Istomin and Leyser, 1998; Mjølhus, 1998) ionospheric conditions), and the profile of the striation
 would be modified by the heating of the plasma.

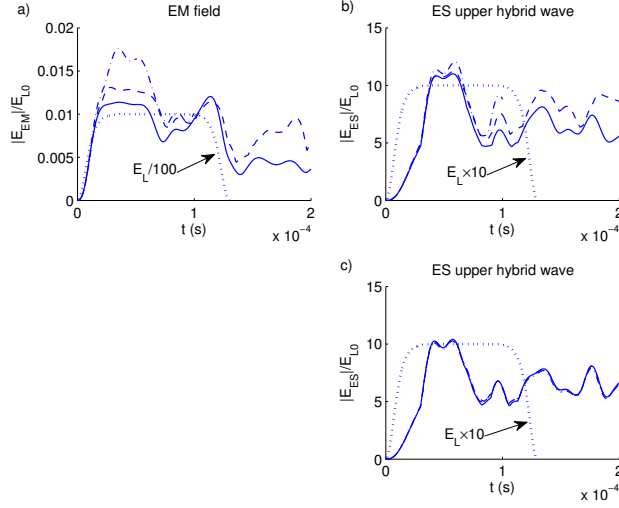


Figure 6. The time development of the amplitudes of the electromagnetic field [panel (a)] associated with Z mode waves and electrostatic field [panel (b)] associated with trapped UH waves, for 1, 7 and 19 deep striations (solid, dashed and dash-dotted lines, respectively) with $\alpha = 0.1$. The amplitude of the external wave electric field \tilde{E}_L is indicated with dotted lines. The results of purely electrostatic simulations are shown in panel (c).

Simulation results using a short driving pulse are shown in Fig. 6 for clusters using 1, 7 and 19 deep striations with $\alpha = 0.1$. In the simulations we use the reference amplitude $\tilde{E}_L = 1 \text{ V/m}$ of the external L mode wave, with a rise time of about 10^{-5} s , indicated with dotted lines in Fig. 6. We choose the pump frequency $\omega_0 = 21.35 \times 10^6 \text{ s}^{-1}$, which is equal to the local UH frequency at the edge of the striation where the plasma density is 95% of the ambient density. A number of different scattering processes (Hall and Leyser, 2003) can be identified in Fig. 6. The L mode is converted to UH waves trapped in the striations, which gives a rapid growth of the electrostatic field in Fig. 6b. As seen in Fig. 6a, the electromagnetic wave amplitude rises initially on the same fast time-scale as the pump wave, which indicates that the pump is also scattered directly to Z mode waves. Visible in Fig. 6b are oscillations in the amplitude of the UH wave with a typical periodicity of $0.5\text{-}1 \times 10^{-4} \text{ s}$. These oscillations are consistent with groups of trapped UH waves being reflected off the edges of the striations. This can be understood by using a one-dimensional ray-tracing picture of the UH wave, whose wave frequency ω and wavenumber k are related through

$$\omega^2 = \omega_{pe}^2 \left(1 + \frac{n_s(x)}{n_0} \right) + \omega_{ce}^2 + 3\kappa v_{Te}^2 k^2 \quad (16)$$

A wavepacket at position $x(t)$ with wavenumber $k(t)$ obeys approximately the equations of motion

$$\frac{dx}{dt} = \frac{\partial \omega}{\partial k} = \frac{3\kappa v_{Te}^2 k}{\omega} \quad (17)$$

$$\frac{dk}{dt} = -\frac{\partial \omega}{\partial x} = -\frac{\omega_{pe}^2}{2\omega n_0} \frac{\partial n_s}{\partial x} = -\frac{\omega_{pe}^2}{2\omega n_0} \frac{\alpha x}{D_{str}^2} \exp\left(-\frac{x^2}{D_{str}^2}\right) \quad (18)$$

This coupled system for the wave packet describes a nonlinear classical oscillator. For small oscillations $x^2/D_{str}^2 < 1$, the equations can be combined to the harmonic oscillator equation

$$\frac{d^2x}{dt^2} = -\Omega^2x \quad (19)$$

where the oscillation frequency is

$$\Omega = \sqrt{3\kappa\alpha} \frac{\omega_{pe}}{\omega} \frac{v_{Te}}{D_{str}}. \quad (20)$$

Using the plasma parameters $v_{Te} = 2.46 \times 10^5$ m/s, $\omega = 21.82 \times 10^6$ s⁻¹, $\kappa = 2.5$, $\alpha = 0.1$ and $D_{str} = 2$ m gives $\Omega = 10^5$ s⁻¹ with a periodicity of $2\pi/\Omega \approx 0.6 \times 10^{-4}$ s. This periodicity is consistent with the typical modulation periods of the UH oscillations in Fig. 6. While there are some small but visible differences in the time-development for different numbers of striations using the fully electromagnetic model in Fig. 6a, b, there is almost no difference between the different cases using the purely electrostatic model in Fig. 6c. Hence, as expected, the coupling between striations is through Z mode radiation.

The Z mode leakage is more significant for shallow striations. Figure 7 shows the amplitudes of the electromagnetic and electrostatic fields for simulations using clusters of 1, 7 and 19 striations having the relative depth $\alpha = 0.01$. The driving frequency $\omega_0 = 21.7858 \times 10^6$ s⁻¹ for the electromagnetic simulations in Figs. 7a,b is near that of the $N = -1$ and $R = 1$ mode in Fig. 2b, which drives the mode resonantly. A purely electrostatic simulation shown as the dotted line in Fig. 7b, d uses a slightly higher frequency of $\omega_0 = 21.799 \times 10^6$ s⁻¹, which drives the purely electrostatic mode resonantly. The main result of the simulations is that a larger number of striations organized in a cluster leads to a larger amplitude of the UH wave. As seen in Fig. 7b, the electrostatic wave amplitude reaches $7E_{L0}$ for 1 striation, $23E_{L0}$ for 7 striations, and $75E_{L0}$ for 19 striations. Hence, the amplitude increases about a factor 3 for each layer of striations in the cluster. The larger amplitudes of the UH oscillations for larger clusters is due to influx of Z mode radiation from neighboring striations within the cluster, which partially compensates the Z mode leakage and leads to a longer confinement time of the wave energy for a larger number of striations in the cluster. For the slightly higher frequency used in Fig. 7c,d, the electrostatic amplitude in Fig. 7d is almost the same as in Fig. 7b for 1 striation, while it is significantly lower in Fig. 7d for the less damped case of 19 striations.

The amplitudes of the electromagnetic wave fields at $t = 5$ ms (Fig. 8) show the influence of groups of shallow striations with $\alpha = 0.01$ on the radiation field. Here the distance between nearest neighbor striations is 24.53 m and the wavelength $\lambda = 2\pi/k$ of the Z mode is estimated using the dispersion relation (15) to be $\lambda \approx 13.46$ m. The most important observation is that for the larger cluster of 19 striations, shown in Fig. 8c, the amplitude of the radiated field is relatively small compared to the field within the cluster of striations.

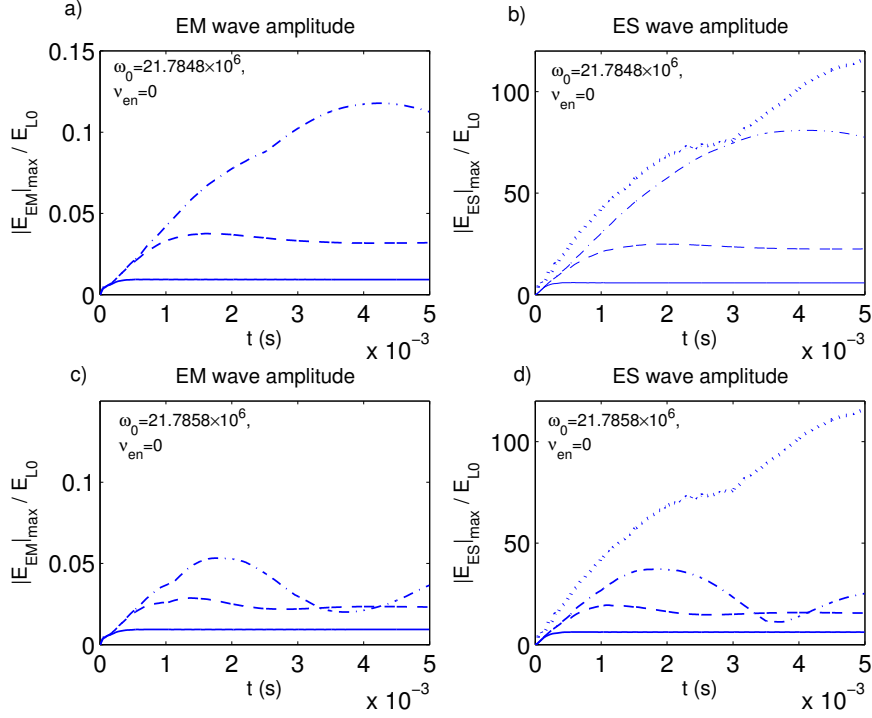


Figure 7. Simulations using shallow striations ($\alpha = 0.01$) and a collision-less model ($\nu_e = 0$) showing the electromagnetic (EM) field amplitude associated with Z mode waves [panels (a) and (c)] and electrostatic (ES) amplitude associated with UH waves [panel (b) and (d)] using a pump frequency of $\omega_0 = 21.7848\text{s}^{-1}$ [panels (a) and (b)] and a slightly higher frequency $\omega_0 = 21.7858\text{s}^{-1}$ [panels (c) and (d)], for 1 striation (solid lines), 7 striations (dashed lines) and 19 striations (dash-dotted lines). The wave frequency for the electromagnetic simulations was set to $\omega_0 = 21.786 \times 10^6 \text{s}^{-1}$. The dotted line in panels (b) and (d) shows the result of an electrostatic simulation on the resonant frequency $\omega_0 = 21.799 \times 10^6 \text{s}^{-1}$, corresponding to the lowest radial mode for $N = -1$ and $R = 1$ in Fig. 2b.

5 Conclusions

340 The mode conversion of an L mode wave to UH waves on small-scale striations has been investi-
 341 gated with numerical simulations. In particular we have addressed how the amplitude of the trapped
 342 UH wave depends on the leakage to Z mode waves escaping the striation. The leakage to Z mode
 343 waves is important for small amplitude striations and may arrest the growth of the striations. The
 344 Z mode leakage is inhibited in groups of striations by multiple scattering of the Z mode wave. In
 345 clusters of striations, the Z mode leakage is inhibited by multiple scattering of the Z mode and UH
 waves on striations. In this case, the UH wave may reach significant amplitude, beyond the threshold
 for parametric instabilities leading to UH and lower hybrid turbulence, and to thermal instabilities
 further enforcing the striations. For large amplitude striations, the mode conversion to UH waves
 is more efficient and the Z mode leakage is less important. In this case the UH amplitude quickly

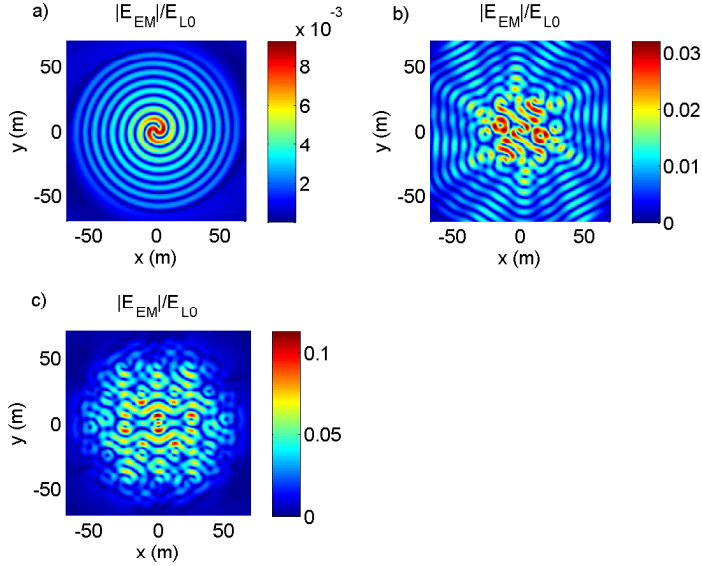


Figure 8. The amplitude of the electromagnetic waves at $t = 5$ ms for different configurations of striations (cf. Fig. 3) for shallow striations with relative depth $\alpha = 0.01$, showing significant Z mode leakage for 1 striation [panel (a)], but less Z mode radiation for 7 striations [panel (b)] and 19 striations [panel (c)]. The separation between nearest neighbor striations is 24.53 m, while the wavelength of the Z mode is $\lambda \approx 13.46$ m.

350 reaches the threshold for nonlinearity and other processes than Z mode leakage become more important. The present study is relevant for ionospheric high frequency pump experiments, where the anomalous absorption of O and L mode waves on field-aligned striations is important and the striations are observed to be clustered in bunches a few hundred meters to kilometers across (Franz et al., 1999; Kosch et al., 2007). The self-consistent formation of clusters of striations and the nonlinear
 355 evolution of the system in the presence of Z mode leakage are interesting questions which we hope to address in future works. In particular, large amplitude UH waves exceeding the threshold for nonlinearity leads to upper hybrid and lower hybrid turbulence (Litvak et al., 1983; Gurevich et al., 1997; Istomin and Leyser, 1998; Mjølhus, 1998), which would dynamically change the spatial profiles of the striations and the resonance conditions for the partially trapped UH waves.

360 Appendix A: Absorbing layer near boundaries

To absorb escaping Z mode waves, an absorbing layer is introduced near the simulation boundaries. A naive implementation by increasing the electron collision frequency ν_e near the boundary in Eq. (6) artificially excites electromagnetic waves near the boundary, since the dipole field $\tilde{\mathbf{E}}_L$ accelerates the electrons, giving a zeroth-order current in the whole simulation domain. Therefore it is desirable
 365 to first eliminate the zero-order current and to localize the external source to the striations, before

introducing the damping. In doing so, we introduce a change of the velocity variable, $\tilde{\mathbf{v}}_e = \tilde{\mathbf{v}}_{e1} + \tilde{\mathbf{v}}_{e0}$, where $\tilde{\mathbf{v}}_{e1}$ is the new velocity variable and $\tilde{\mathbf{v}}_{e0}$ is the zeroth order electron velocity, defined via

$$i\omega_0 \tilde{\mathbf{v}}_{e0} - \frac{e}{m_e} \left(\tilde{\mathbf{E}}_L + \tilde{\mathbf{v}}_{e0} \times \mathbf{B}_0 \right) - \nu_e \tilde{\mathbf{v}}_{e0} = 0. \quad (\text{A1})$$

In this manner, the external source $\tilde{\mathbf{E}}_L$ is eliminated from Eq. (6), which now reads

$$370 \quad \frac{\partial \tilde{\mathbf{v}}_{e1}}{\partial t} = i\omega_0 \tilde{\mathbf{v}}_{e1} - \frac{e}{m_e} \left(\tilde{\mathbf{E}} + \tilde{\mathbf{v}}_{e1} \times \mathbf{B}_0 \right) - \frac{3v_{Te}^2}{n} \kappa \nabla \tilde{n}_e - \nu_e \tilde{\mathbf{v}}_{e1}, \quad (\text{A2})$$

and new source terms via $\tilde{\mathbf{v}}_{e0}$ are instead introduced into Eqs. (3) and (5), giving

$$\frac{\partial \tilde{\mathbf{E}}_{EM}}{\partial t} = i\omega_0 \tilde{\mathbf{E}}_{EM} - c^2 \nabla^2 \tilde{\mathbf{A}} - \frac{e}{\varepsilon_0} \nabla^{-2} \nabla \times \{ \nabla \times [n(\tilde{\mathbf{v}}_{e1} + \tilde{\mathbf{v}}_{e0})] \}, \quad (\text{A3})$$

and

$$\frac{\partial \tilde{n}_e}{\partial t} = i\omega_0 \tilde{n}_e - \nabla \cdot [n(\tilde{\mathbf{v}}_{e1} + \tilde{\mathbf{v}}_{e0})], \quad (\text{A4})$$

375 respectively. Solving for $\tilde{\mathbf{v}}_{e0}$ in Eq. (A1) gives

$$\tilde{\mathbf{v}}_{e0} = - \frac{1}{(\omega_0 + i\nu_e)^2 - \omega_{ce}^2} \frac{e}{m_e} \left[i(\omega + i\nu_e) \tilde{\mathbf{E}}_L + \frac{e}{m_e} \tilde{\mathbf{E}}_L \times \mathbf{B}_0 \right]. \quad (\text{A5})$$

The source terms are now effectively localized around the striations, since the spatial derivatives of $n\tilde{\mathbf{v}}_{e0}$ in the right-hand sides of Eqs. (A3) and (A4) vanish far away from the striations. As a last step, the collision frequency ν_e is increased near the boundaries only in the momentum equation (A2). In the simulations of the electromagnetic model, a term $\omega_0 \exp[-(r - L_x/2)^2/15^2]$ for $r < L_x/2$ and ω_0 for $r \geq L_x/2$ is added to ν_e in Eq. (A2), where $r = \sqrt{x^2 + y^2}$ is the radial coordinate and L_x is the width of the simulation domain.

Appendix B: Calculation of resonance frequencies and profiles of trapped UH waves

To calculate the resonance frequencies in Fig. 1b,c and 2b,c for different azimuthal and radial modes of the system (9)–(10) or of Eq. (13), we rewrite Eqs. (9)–(10) as

$$\frac{1}{r} \frac{\partial}{\partial r} \left(r \frac{\partial \tilde{\Phi}}{\partial r} \right) - \frac{N^2}{r^2} \tilde{\Phi} - \frac{\omega_{pe}^2}{3v_{Te}^2 \kappa} \left(\frac{n}{n_0} - 1 \right) \tilde{\Phi} - \frac{\omega^2}{3v_{Te}^2 \kappa} \tilde{\Psi} - \lambda = 0, \quad (\text{B1})$$

$$\frac{1}{r} \frac{\partial}{\partial r} \left(r \frac{\partial \tilde{\Psi}}{\partial r} \right) - \frac{N^2}{r^2} \tilde{\Psi} + \frac{X}{r^2} \left(r \frac{\partial}{\partial r} - YN \right) \left(\frac{r}{n_0} \frac{\partial n}{\partial r} \tilde{\Phi} \right) - \frac{(\omega^2 - \omega_{pe}^2 - \omega_{ce}^2)}{3v_{Te}^2 \kappa} - \lambda = 0, \quad (\text{B2})$$

and Eq. (13) as

$$390 \quad \frac{1}{r} \frac{\partial}{\partial r} \left(r \frac{\partial \tilde{\Phi}}{\partial r} \right) - \frac{N^2}{r^2} \tilde{\Phi} - \frac{\omega_{pe}^2}{3v_{Te}^2 \kappa} \left(\frac{n}{n_0} - 1 \right) \tilde{\Phi} - \lambda = 0, \quad (\text{B3})$$

where $\lambda = -\omega^2(1 - X - Y^2)/(3v_{Te}^2 \kappa) = -(\omega^2 - \omega_{pe}^2 - \omega_{ce}^2)/(3v_{Te}^2 \kappa)$ is treated as an eigenvalue of the system. Once λ is found, the wave frequency is obtained as $\omega = \sqrt{\omega_{pe}^2 + \omega_{ce}^2 - 3v_{Te}^2 \kappa \lambda}$. The

two last terms in the left-hand side of Eq. (B2), which will add up to zero, have been added to cast Eq. (B2) as an eigenvalue problem of the same form as Eq. (B1).

395 The next step is to convert the ordinary differential equations into coupled algebraic equations, which is done by discretizing the variables $\tilde{\Phi}$ and $\tilde{\Psi}$ on an equidistant grid $r = r_j = j\Delta r$ with $j = 0, 1, \dots, M$ and grid size Δr , such that $\tilde{\Phi}(r_j) \approx \tilde{\Phi}_j$ and $\tilde{\Psi}(r_j) \approx \tilde{\Psi}_j$, and using centered difference approximations of the spatial derivatives, for example $\partial\tilde{\Phi}/\partial r \approx (\tilde{\Phi}_{j+1} - \tilde{\Phi}_{j-1})/(2\Delta r)$ and $\partial^2\tilde{\Phi}/\partial r^2 \approx (\tilde{\Phi}_{j+1} - 2\tilde{\Phi}_j + \tilde{\Phi}_{j-1})/\Delta r^2$. Typical numerical parameter values used were $M = 400$
400 and $\delta r = 0.1$ m. The boundary conditions for $N \neq 0$, e.g. $\tilde{\Phi}_0 = 0$, $\tilde{\Psi}_0 = 0$, $\tilde{\Phi}_M = 0$, and $\tilde{\Psi}_M = 0$ are used to eliminate $\tilde{\Phi}_0$, $\tilde{\Psi}_0$, $\tilde{\Phi}_M$, and $\tilde{\Psi}_M$ from the system. The continuous boundary value problems are then converted into standard matrix eigenvalue problems of the form $(A - \lambda I)V = 0$, where A is a sparse matrix representing an approximation of the differential equations, λ is the eigenvalue, I is the unit matrix, and V is the eigenvector containing $\tilde{\Phi}_j$ and $\tilde{\Psi}_j$. For the system (B1)–(B2) the unknowns
405 are organized as a column vector $V = [\tilde{\Phi}_1 \tilde{\Psi}_1 \tilde{\Phi}_2 \tilde{\Psi}_2 \dots \tilde{\Phi}_{M-1} \tilde{\Psi}_{M-1}]^T$ (where T denotes the transpose of the matrix) and for Eq. (B3), the unknowns are organized as $V = [\tilde{\Phi}_1 \tilde{\Phi}_2 \dots \tilde{\Phi}_{M-1}]^T$. The system has in total $M - 1$ eigenvalues and eigenvectors, but eigenvalues that are of interest are only those that are real-valued and positive, which give oscillation frequencies ω smaller than the ambient UH frequency and to trapped UH waves. The eigenvalue problem can be solved numerically with
410 any standard package: We used Matlab's 'eigs' function, which gives both the eigenvalues and the corresponding eigenvectors. For Eq. (B3), a numerical solution of the eigenvalue problem gives immediately the frequencies of the trapped eigenmodes. For the system (B1)–(B2), an approximation of ω is first given as a starting estimate, which is used to calculate the values of X and Y , after which the eigenvalue problem is solved to find λ for the mode of interest. Then λ is used to calculate a new
415 value of ω , and the process is repeated until convergence.

For the particular case of purely radial oscillations with $N = 0$, Eq. (B3) was solved as it stands, whole we replaced Eq. (B2) by Eq. (12) to eliminate $\tilde{\Psi}$ in Eq. (B1). The integral was approximated with the trapezoidal rule $\int_r^\infty f dr \approx (f_j/2 + f_{j+1} + f_{j+2} + \dots + f_{M-1})\Delta r$, where $f_j \approx f(r_j) = (X/n_0)[(\partial n/\partial r)\tilde{\Phi}]_{r=r_j}$. The approximation of the boundary condition at $r = 0$, $\partial\tilde{\Phi}/\partial r \approx (\tilde{\Phi}_1 - \tilde{\Phi}_0)/\Delta r = 0$, was used to eliminate $\tilde{\Phi}_0$ from the system.
420

Acknowledgements. B. E. acknowledges support from the Engineering and Physical Sciences Research Council (EPSRC), U.K., Grant no. EP/M009386/1.

References

- Cohen, R. and Whitehead, J. D.: Radio-reflectivity detection of artificial modification of the ionospheric F layer, *J. Geophys. Res.*, 75(31), 6439–6445, doi:10.1029/JA075i031p06439, 1970.
- 425 Dysthe, K. B., Mjølhus, E., Pécseli, H., and Rypdal, K.: Thermal cavitons, *Phys. Scr.*, T2/2, 548–559, 1982.
- Eliasson, B.: Full-scale simulations of ionospheric Langmuir turbulence, *Mod. Phys. Lett. B*, 27(8), 1330005, doi:10.1142/S0217984913300056, 2013.
- Eliasson, B. and Papadopoulos, K.: Numerical study of anomalous absorption of O mode waves on magnetic field-aligned striations, *Geophys. Res. Lett.* **42**, 2603–2611, doi:10.1002/2015GL063751, 2015.
- 430 Franz, T. L., Kelley, M. C., and Gurevich, A. V.: Radar backscattering from artificial field-aligned irregularities, *Radio Sci.*, 34(2), 465–475, 1999.
- Gurevich, A. V., Zybin, K. P., and Lukyanov, A. V.: Stationary Striations Developed in the Ionospheric Modification, *Phys. Rev. Lett.*, 75, 2622–2625, 1995a.
- 435 Gurevich, A. V., Zybin, K. P., and Lukyanov, A. V.: Stationary state of isolated striations developed during ionospheric modification, *Phys. Lett. A*, 206, 247–259, 1995b.
- Gurevich, A. V., Lukyanov, A. V., and Zybin, K. P.: Anomalous absorption of powerful radio waves on the striations developed during ionospheric modification, *Phys. Lett. A*, 211, 363–372, 1996.
- Gurevich, A. V., Carlson, H., Lukyanov, A. V., and Zybin, K. P.: Parametric decay of upper hybrid plasma waves trapped inside density irregularities in the ionosphere, *Phys. Lett. A*, 231, 97–108, 1997.
- 440 Gurevich, A., Hagfors, T., Carlson, H., Karashtin, A., and Zybin, K.: Self-oscillations and bunching of striations in ionospheric modifications, *Phys. Lett. A*, 239, 385–392, 1998.
- Hall J.-O. and Leyser, T. B.: Conversion of trapped upper hybrid oscillations and Z mode at a plasma density irregularity, *Phys. Plasmas*, 10, 2509–2518, 2003.
- 445 Hall, J.-O., Istomin, Y. N., and Leyser, T. B.: Electromagnetic coupling of localized upper hybrid oscillations in a system of density depletions, *Phys. Plasmas*, 16, 012902, 2009.
- Inhester, B., Das, A. C., and Fejer, J. A.: Generation of small-scale field-aligned irregularities in ionospheric heating experiments, *J. Geophys. Res.*, 86, 9101–9106, 1981.
- Istomin, Y. N. and Leyser, T. B.: Small-scale magnetic field-aligned density irregularities excited by a powerful electromagnetic wave, *Phys. Plasmas*, 4, 817–828, 1997.
- 450 Istomin, Y. N. and Leyser, T. B.: Parametric interaction of self-localized upper hybrid states in quantized plasma density irregularities, *Phys. Plasmas*, 5, 921–931, 1998.
- Istomin, Y. N., Hall, J.-O., and Leyser, T. B.: Electromagnetic interaction of localized upper hybrid oscillations in a system of density depletions, *Adv. Space Res.*, 38, 2516–2517, 2006.
- 455 Istomin, Ya. N. and Leyser, T. B.: Enhanced nonlinear interaction of powerful electromagnetic waves with ionospheric plasma near the second electron gyroharmonic, *Phys. Plasmas*, 20(5), 052904, 2013.
- Kelley, M. C., Arce, T. L., Salowey, J., Sulzer, M., Armstrong, W. T., Carter, M., and Duncan, L.: Density depletions at the 10-m scale induced by the Arecibo heater: *J. Geophys. Res.*, 100(A9), 17367–17376, doi:10.1029/95JA00063, 1995.
- 460 Kosch, M. J., Pedersen, T., Mishin, E., Starks, M., Gerken-Kendall, E., Sentman, D., Oyama, S., and Watkins, B.: Temporal evolution of pump beam self-focusing at the High-Frequency Active Auroral Research Program, *J. Geophys. Res.*, 112, A08304, 10.1029/2007JA012264, 2007.

- Leysner, T. B. and Nordblad, E.: Self-focused radio frequency L wave pumping of localized upper hybrid oscillations in high-latitude ionospheric plasma, *Geophys. Res. Lett.*, 36, L24105, 10.1029/2009GL041438, 465 2009.
- Litvak, A. G., Petrukina, V. I., Sergeev, A. M., and Zhislin, G. M.: Dynamics of one-dimensional upper-hybrid turbulence in a magnetized plasma, *Phys. Lett. A*, 94, 85–88, 1983.
- Lominadze, D. G.: *Cyclotron Waves in Plasmas*, Pergamon Press, New York, 1981.
- Mjølhus, E.: On reflexion and trapping of upper-hybrid waves, *J. Plasma Phys.*, 29, 195–215, 1983.
- 470 Mjølhus, E.: Anomalous absorption and reflection in ionospheric radio modification experiments, *J. Geophys. Res.*, 90(A5), 4269–4279, doi:10.1029/JA090iA05p04269 (1985).
- Mjølhus, E.: Theoretical model for long time stimulated electromagnetic emission generation in ionospheric radio modification experiments, *J. Geophys. Res.*, 103 (A7), 14711–14729, 1998.
- 475 Stubbe, P., Kopka, H., Jones, T. B., and Robinson, T.: Wide band attenuation of radio waves caused by powerful HF waves: Saturation and dependence on ionospheric variability, *J. Geophys. Res.*, 87(A3), 1551–1555, doi:10.1029/JA087iA03p01551, 1982.
- Vas'kov, V. V. and Gurevich, A. V.: Nonlinear resonant instability of a plasma in the field of an ordinary electromagnetic wave, *Sov. Phys. JETP, Engl. Transl.*, 42, 91–97, 1976.
- 480 Vas'kov, V. V. and Gurevich, A. V.: Amplification of resonant instability and generation of wideband radio emission by high-power radio waves incident on the ionosphere, *Geomagn. Aeron.*, 24, 350–356, 1984.